Journal of the Korean Society
for Nondestructive Testing
Vol. 26, No. 3 (2006. 6)

A Simulation Tool for Ultrasonic Inspection

Adarsh Krishnamurthy*, K.V. Mohan*, Soumya Karthikeyan*,
C.V. Krishnamurthy*,† and Krishnan Balasubramaniam*

Abstract A simulation program SIMULTSONIC is under development at CNDE to help determine and/or help optimize ultrasonic probe locations for inspection of complex components. SIMULTSONIC provides a ray-trace based assessment for immersion and contact modes of inspection. The code written in Visual C++ operating in Microsoft Windows environment provides an interactive user interface. In this paper, a description of the various features of SIMULTSONIC is given followed by examples illustrating the capability of SIMULTSONIC to deal with inspection of canonical objects such as pipes. In particular, the use of SIMULTSONIC in the inspection of very thin-walled pipes (with 450 um wall thickness) is described. Ray trace based assessment was done using SIMULTSONIC to determine the standoff distance and the angle of oblique incidence for an immersion mode focused transducer. A 3-cycle Hanning window pulse was chosen for simulations. Experiments were carried out to validate the simulations. The A-scans and the associated B-Scan images obtained through simulations show good correlation with experimental results, both with the arrival time of the signal as well as with the signal amplitudes.

Keywords: Ultrasonic Inspection, Simulation, Ray-Tracing
PACS 43.35 Cg, 43.38 Hz

1. Introduction

Ultrasonic inspection of a component for flaw detection is a routine requirement in the industry. When the component shapes are simple (flat or locally flat surfaces, large cylindrical surfaces etc), inspectability can be determined from a combination of well-known thumb rules arrived at through field experience and standard physical laws such as the Snell's law. For complex shapes of the components, inspectability becomes a non-trivial task due to the complex ways by which ultrasonic waves propagate through and interact with interfaces and/or surfaces. Three frequently encountered problems are (a) to determine "lit" and "shadow" regions within the component, (b) to identify flaw signals among the various signals that constitute an A-scan and (c) to solve for the scan path a probe/detector should adopt to "image" the flaw. The first problem needs to be solved to ensure that the flaw is insonified for some probe/detector orientation and separation. The second problem needs to be solved to extract the flaw signal from the "noise" generated by the complex shape of the component. Determination of the scan path requires the solutions to the first two problems. Inspectability therefore requires an assessment of the transducer field patterns within the inspection volume of a component. While a quantitative assessment is desirable, even a qualitative assessment when combined with visualization would prove valuable.

Beam models have been and are being developed to predict transducer field patterns in

Received: November 7, 2005, Accepted: March 9, 2006. * Centre for Nondestructive Evaluation, Department of Mechanical Engineering, Indian Institute of Technology, Madras Chennai 600 036, Tamil Nadu, India,
† Corresponding author: cvkmind2003@yahoo.com

single media and in cases involving two media separated by a flat or curved surface (Goswami et al, 1991; Gengembre and Lhemery, 2000; Schmerr et al, 1994; Ginzel and Hotchkiss, 1997; Schmerr, 1998, 2000; Krishnamurthy et al, 2005). These models become computationally intensive for complex shaped component geometries. Ray based assessment is an attractive alternative as it provides a quick and intuitive assessment of arrival times and coverage to aid our understanding of wave propagation in complex component geometries. A ray picture for a specific source-object-receiver configuration, however qualitative, is a very useful construct (Adarsh et al, 2003). With the advent of high-end desktop computers, a quantitative assessment of a ray picture has been made possible which has provided good results often with surprising accuracy. There have been many areas ranging from optics, to radiowave communication (Rossi and Levy, 1992), to underwater acoustics (Porter 1997) where the ray picture has provided simple, intuitive and reasonably correct assessment. Even in ultrasonic non-destructive evaluation, several ray-based assessments have been and are being developed (Schmerr, 1998). Prediction of the time-of-arrival of a pulse, the distinction between longitudinal and shear wave arrivals, the identification of mode converted signals and the determination of "lit" and "shadow" regions are important features that a ray picture can provide with reasonable accuracy. While it is known that rays cannot model diffraction effects, it is a well-established practice to combine the results from geometric theory of diffraction (GTD) with the ray picture to provide a reasonable model of diffraction phenomena (Achenbach et al, 1982).

At CNDE, as part of a large research program, the need to develop a ray-based assessment code for UT inspection is being addressed through a simulation program SIMULTSONIC (Adarsh et al, to be published). The code is designed to describe pulse propagation characteristics directly in time domain through a ray picture. It is written in Visual C++ operating in Microsoft Windows environment and provides an interactive user interface. It employs a time-stepping scheme to launch rays from the transducer, traces its path to the nearest interface, generates new rays at the interface satisfying Snell's law, tracks mode conversion all in a recursive manner. Immersion and contact modes of inspection are available in SIMULTSONIC.

2. Ray Model

Each ray is characterized by the position of its head, which is given by the global X, Y and Z coordinates. The ray also has three direction cosines that describe the direction in which the ray propagates. Each ray is also characterized by its type (whether shear or longitudinal) and its energy. The ray also has information about the amount of time lapsed from the time it was created at the transducer. The rays are generated as a parallel, converging or diverging beam from the transducer as shown in Fig. 1.

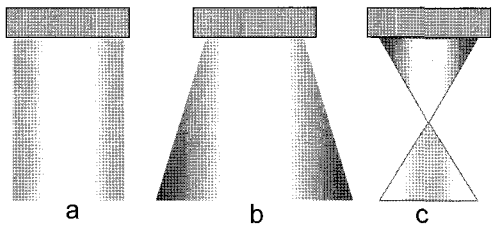

Fig. 1 Cylindrical (a), Diverging (b) and Converging (c) Beams from a Transducer

Ray tracing is carried out in specific time steps and checks are made at every stage to ascertain the ray position in the domain as a function of the time elapsed. Each ray is propagated until it meets an interface or has reached the end of the domain or until the given time. Once a ray meets an interface, new reflected and refracted rays are created based on the angle of incidence of the rays taking into account mode conversion. Generation of the

reflected ray or the refracted ray is also governed by the critical angles, evaluated using the sound speeds in the two media. In the most general case (a solid-solid interface with incident angle below the first critical angle), four new rays are formed. These are the shear reflected and refracted rays and the longitudinal reflected and refracted rays. The incident ray can be either a shear ray or a longitudinal ray. Fig. 2 represents the basic reflection and refraction processes at an interface between two media. The incident plane wave is described in terms of a ray defined by the unit vector $\hat{e}$, the reflected plane wave by a ray with unit vector $\hat{r}_1$, and the refracted plane wave by a ray with unit vector $\hat{r}_2 \cdot \hat{n}$ denotes the normal at the interface.

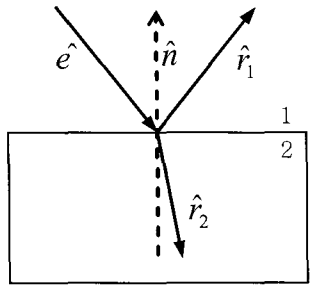

Fig. 2 The schematic represents the basic refraction and reflection process at an interface between media

$$\frac{\sin \varphi^{m}{}_{P,SV}}{c^{m}{}_{P,SV}} = \text{constant} \quad m = 1,2 \tag{1}$$

$$\hat{r}_1 = \hat{e} + 2(-\hat{e} \cdot \hat{n})\,\hat{n} \tag{2}$$

$$\hat{r}_2 = \left(\frac{c_2}{c_1}\right)\hat{e} + \left[\left(\frac{c_2}{c_1}\right)(-\hat{e} \cdot \hat{n}) + \sqrt{1 + \left(\frac{c_2}{c_1}\right)^2 ((-\hat{e} \cdot \hat{n})^2 - 1)}\right]\hat{n} \tag{3}$$

Eqn. (1) represents the generalized Snell's law in which $c^{m}{}_{P,SV}$ represents the velocity of the corresponding mode and φ represents the angle that the ray makes with the normal. Using the generalized Snell's law given by eqn. (1) and the law of reflection and refraction (Incident ray, reflected ray or transmitted ray and the normal at the point of contact lie in the same plane), the vectors of the reflected and refracted ray are calculated as shown in.

Eqn. (2) give the expressions for the reflected ray in terms of the incident ray and the normal at the point of contact assuming no mode conversion. Eqn. (3) describes the refraction process at a fluid-solid interface with c_2 taking the possible combinations of *P-P*, and *P-SV* waves or *SV-SV*, and *SV-P* waves.

The standoff distance of the transducer from the surface of the specimen is initially determined by shooting a single central ray to an object/ interface. The beam model is then invoked to generate either a diverging beam or a cylindrical beam depending on the standoff distance. If a focused transducer is used then a focused beam is produced. Using the normal at the transducer face and a unit vector perpendicular to it, the direction of the rays originating from the transducer is found from vector algebra. The rays are created at the apparent origin and their origin is shifted along their direction of propagation to start from the face of the transducer. For cylindrical rays, the ray origin is shifted along this vector based on the distance required from the center of the transducer.

3. Beam Model

The peak-to-peak RF pulse amplitudes associated with the rays generated from a planar transducer is governed by an approximate beam model. The model is based on the exact on-axis variation and the exact cross-axis distribution corresponding to the centre frequency of the bandwidth of the pulse. The on-axis and the cross-axis distributions are chosen to be beyond the characteristic near-field to far-field transition distance $N=a^2/\lambda$ corresponding to the wave length (λ) at the specified central frequency and radius (a) of a circular transducer. Fig. 3 depicts the on-axis variation of the normalized pressure, in

the frequency domain, with three distance regions marked. Eqn. (4) gives the closed form equation of the on-axis pressure distribution.

$$\frac{p(z,\omega)}{\rho c v_o} = \left[\exp(ikz) - \exp(ik\sqrt{z^2 + a^2}) \right] \quad (4)$$

In Region I, the peak-to-peak amplitude of rays are taken to be independent of distance since for a pulse of finite bandwidth, the on-axis contributions due to all the frequency components average out. Further, the cross-axis distribution is taken to be uniform in Region I, constrained only by energy conservation, leading to a non-diverging cylindrical beam of diameter equal to that of the transducer. In Region III, the peak-to-peak amplitude distribution follows an approximate Gaussian function that is matched to the 6 dB points of the exact cross-axis distribution corresponding to the centre frequency of the bandwidth of the pulse.

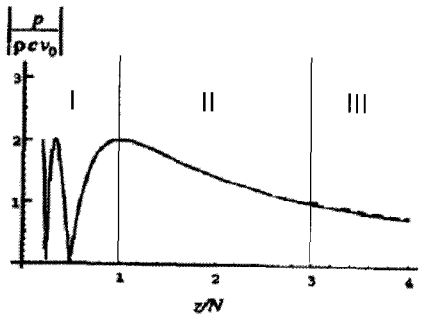

Fig. 3 On-axis variation of the normalized pressure. The program employs the three marked regions for assigning the appropriate amplitude distribution for the rays.

Region II is a transition region and is modeled by a Gaussian distribution whose central maximum follows the exact on-axis variation with the cross-axis variation constrained by energy conservation. The distribution is matched with Region I and Region III distributions such that the exact on-axis variation, corresponding to the centre frequency of the pulse bandwidth, is followed throughout. In Regions II and III, a single diverging beam is generated to approximate the main beam of a planar transducer. In the model, the divergent beam is generated from an apparent beam origin located behind the face of the transducer as shown in Fig. 4. Its location is determined as given by eqn. (5) from the near-field distance $(4a^2-\lambda^2)/4\lambda$, and the half angle of divergence γ based on the 6 dB drop calculated from the well-know relation (Krautkrä mer, 1990) $\sin\gamma = K_{6dB}\ (\lambda/a)$ where $K_{6dB} = 0.35$.

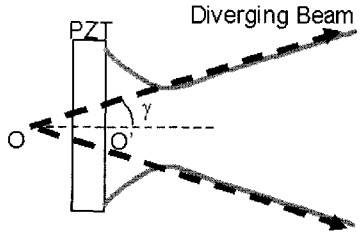

Fig. 4 Representation of Beam Divergence - the 6 dB field contour (in grey) is modeled by the cone (in black dotted line) originating from an apparent origin O that is situated behind the transducer face centre O'.

$$OO' = \frac{4a^2 - \lambda^2}{4\lambda} - a\frac{\sqrt{4a^2 - K_{6dB}^2\lambda^2}}{K_{6dB}\lambda} \quad (5)$$

The beam model for a spherically focused transducer is constructed in a similar manner based on the corresponding on-axis variation. The cross-axis variation at the focal plane is taken as the characteristic feature and an approximate Gaussian function is determined resulting in a single converging beam.

4. Program Capabilities

The program provides an interactive display of the geometrical features of the object and of the transducer location and orientation. The user can locate and orient the transducer at any desired position with respect to the object. The user can also specify the scan path of the transducer relative to the object. The program allows for generation of simple canonical object shapes and provides for import of more complex

object geometries from standard packages such as ANSYS™. The program can simultaneously display the inspection configuration and the corresponding A-scan. It is possible to define a scan profile and export the data for generating B-scan displays. Currently, the program provides for conventional planar and spherically focused circular transducers and a linear phased array.

5. B-Scan Simulation with Conventional Transducer

Fig. 5 illustrates the B-scan feature of the software 6.35 mm diameter, 5 MHz central frequency, circular planar immersion transducer was moved at a constant height of 127 mm above an 83.8 mm diameter solid cylinder. A beam spread of 5° was assumed. In Fig. 5, the panel on the left depicts the configuration and the instantaneous position of the transducer corresponding to B-scan immersion mode of inspection over a solid cylinder under normal incidence.

6. B-Scan with Phased Array-Simulation and Validation

Linear phased array probes are modeled by combining rays from individual elements of the array with suitable time delay laws corresponding to beam steering and/or beam focusing.

Fig. 6 shows the simulated and experimental B-Scan of a 6 mm notch in an 11 mm thick plate.

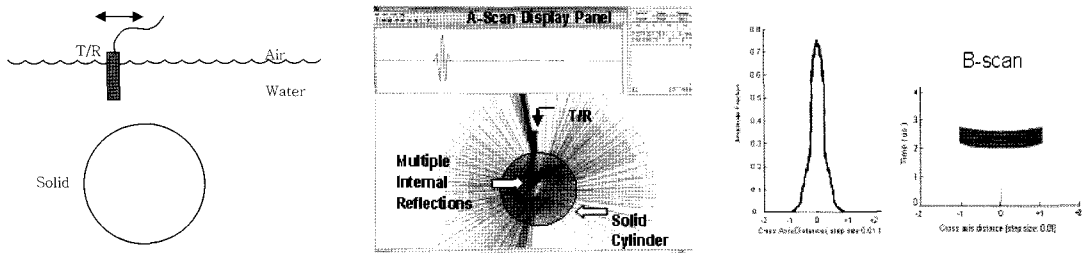

Fig. 5 The schematic is shown at top left. The top right panel shows the A-scan and a snap shot of rays undergoing multiple refraction and internal reflections due to the cylinder. The peak-to-peak amplitude response for the B-scan is shown in the lower left panel. The cylinder diameter extends from -3.3 to +3.3 on the x-axis scale. The lower right panel is a zoomed section of the B-scan.

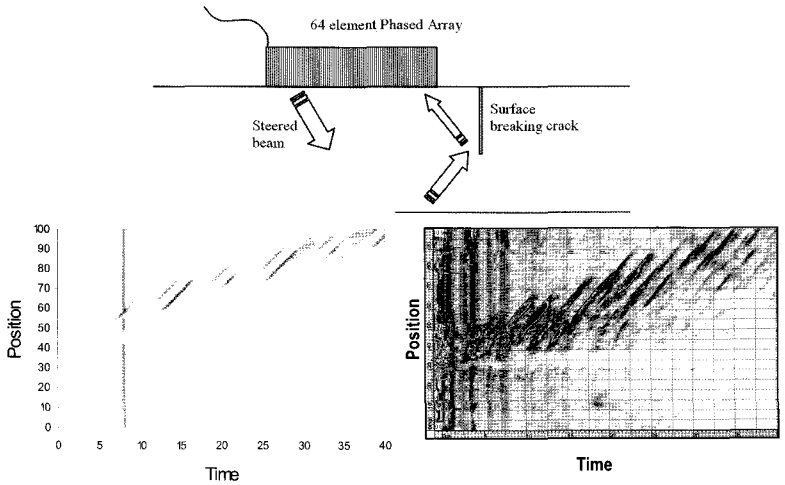

Fig. 6 The schematic of the phased array inspection of the thick section is depicted at the top panel. Simulated (lower left panel) and Experimental (lower right panel) Phased Array B-Scan of a 6mm deep surface-breaking notch in an 11 mm thick plate. When superposed, the correspondence between simulation and experiment is very good.

The scan was done using a 5 MHz transducer with a 45° beam steering. The experiment was carried out using OMNISCAN phased array module from RD Tech.

7. Pipe Inspection Simulation

SIMULTSONIC can internally generate simple shapes such as cylinders or pipes. Flaw detection and characterization, even in such simple shapes, depends very much on probe location and orientation and is controlled by the pipe dimensions and flaw orientation. Often, mode conversion can lead to complex signals that are difficult to interpret. Simulation is an economic alternative that can assist in identifying optimum probe positions and help interpret complex signals. Fig. 7 shows the schematic of an 11 mm thick pipe of large radius of curvature with an 8 mm EDM notch of 1.5 mm width. The pipe is considered immersed in water and the material of the pipe is taken to be steel.

The simulation is carried out on a region around the notch location approximated as a flat section due to the large curvature of the pipe. The EDM notch is modeled as surface opening cuboid. The simulations were carried out for various probe angles. Mode converted signals can be seen for the probe angle at 8°. Probe angles of 12° or more appears to be well suited for detection of a vertical notch. As the first critical angle is at 13°, there is only one flaw signal for the probe angle of 14°, whereas there are two signals, one each from the shear and longitudinal waves for the probe angle of 12°.

8. Thin Pipe Inspection-Simulation and Validation

Optimization of the parameters for the inspection of a weld between two sections of a thin-walled pipe is the final example to be discussed in this paper. The pipe is a thin walled stainless steel cylinder with a wall thickness of 0.4 mm and an outer diameter of 6.5 mm. Access is confined to only one section of the pipe and hence to only one side of the weldment. The weld region, a few hundred microns thick, is assumed isotropic. Given the constraints of the problem, a 12.7 mm diameter, 15 MHz immersion transducer with a spherical focal length of 38.1 mm, in water, was chosen for the task. An angle-beam inspection with shear waves was envisaged.

Simulations were carried out to find the optimum standoff distance as well as the optimum angle of inspection. The distance of the center of the probe from the wall to be welded was maintained as 38.1mm, to keep the wall in focus, and the probe angle was varied from 16° to 23°. Fig. 8 shows the variation of the received energy with respect to transducer position as well as the transducer angle.

From the results obtained by simulations, the

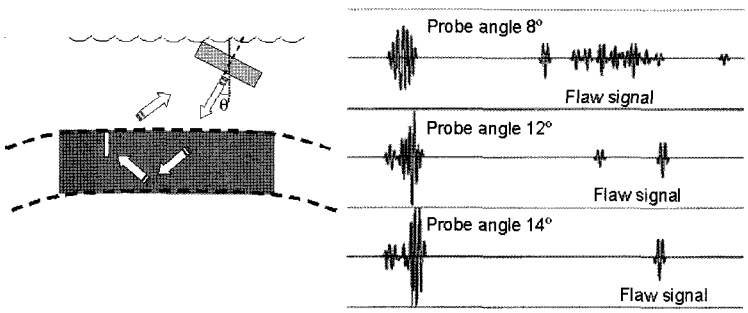

Fig. 7 Simulation of the inspection, under immersion, of 8 mm long notch in an 11 mm thick pipe with a large radius of curvature. The transducer was taken to be 12.7 mm diameter with 5 MHz centre frequency. The schematic of the configuration is shown on the left. Simulated A-scans for various probe angles are shown on the right. At a probe angle of 14° in water, a clear S-wave flaw signal can be seen.

probe angle was chosen to be 19°, and the standoff distance was chosen to be 12 mm along the pipe axis with a corresponding vertical standoff distance of 35 mm. An experiment was setup to validate the results experimentally.

Fig. 9 shows the pipe holder with supports, the XY-scanner, the probe in a manipulator and the immersion tank.

The pipe is mounted on two bushes to prevent wobble as it is rotated. A Lab-View program was written to control the angular position of the tube, to control the probe fixed to the XY-scanner and for data acquisition. The probe manipulator was used to change the probe angle manually. The 15 MHz spherically focused transducer was powered by a Panametrics PR500 pulser-receiver. The signal was sampled at 100 MHz.

Fig. 10 shows the B-scans obtained from the experiment and simulation.

The images show good correlation both with the arrival time of the signal as well as the amplitudes of the signals. It can be seen that as the position of the transducer is moved farther from the pipe wall the arrival time increases and the amplitude of the received signal also drops.

It is also verified that the signal received is maximum at around 11-13 mm that was predicted during the initial studies.

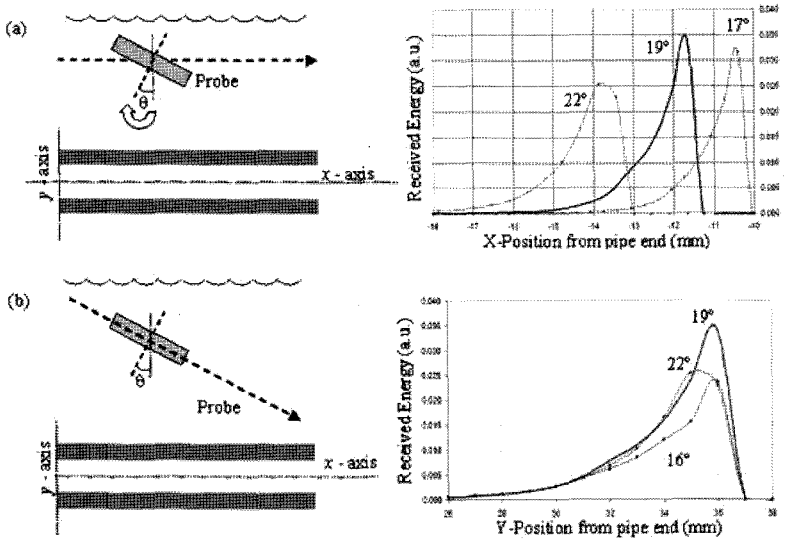

Fig. 8 Simulation to determine optimum location and orientation of a focused probe. (a) received energy as the probe was moved along the x-axis. The schematic is shown on the left. (b) the schematic on the left shows the probe scan path in the xy plane. On the right, the received energy as the probe was moved along the y-axis.

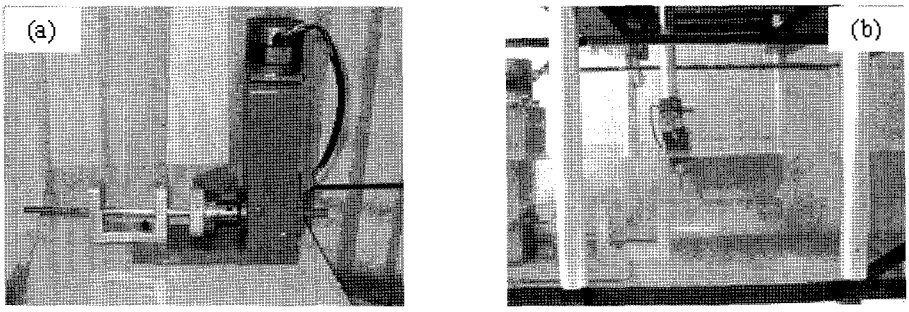

Fig. 9 (a) Tube holder with a stepper motor, (b) probe manipulator mounted on a XY-scanner

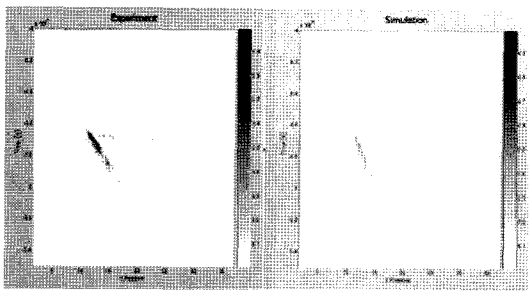

Fig. 10 B-scans obtained from experiment (left panel) and simulations (right panel)

Fig. 11 shows the sum of the peak-to-peak amplitudes obtained from simulation as well as experiments as a function of probe position. The results obtained from experiments confirm the validity of the simulations.

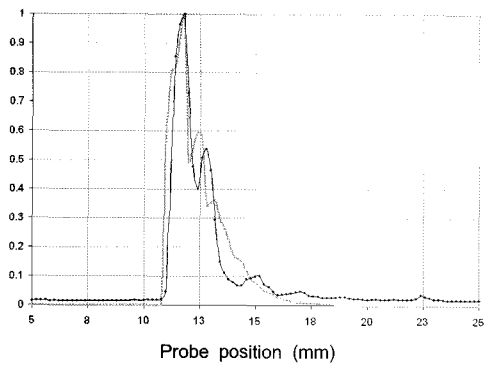

Fig. 11 Measured (curve in black with dots) and simulated (curve in grey) variation of the normalized received energy with probe position. The increase in amplitude at around 14 mm is noted both in experiments as well as in simulations.

9. Summary and Conclusions

SIMULTSONIC makes visualization of the insonified regions possible. Simple beam models provide a reasonable representation for circular planar and spherically focused transducers. A-scans and B-scans can be generated. SIMULTSONIC handles canonical geometries and supports import of surface meshes. The interactive GUI helps the user to specify/modify probe and object locations as well as to define probe scan paths. Delay laws for beam steering in linear phased arrays have been developed and validated with a phased array system. Simulations on a thin pipe using a conventional focused transducer have been validated.

On-going work includes providing a facility to import files made with graphic packages (e.g., ProE, UG) to represent components with complex geometries, incorporating GTD for crack response, and providing field calculations in specific cases.

References

Achenbach, J. D., Gautesen, A. K. and McMaken, H. (1982) Ray Methods for Waves in Elastic Solids, Pitman Books Ltd.

Adarsh, K., Dewangan, S., Rangan, B. and Katragadda, G. (2003) Generic Ultrasonic 3D Ray Tracing Incorporating Beam Energy Models, *Review of Progress in Quantitative Non Destructive Evaluation*, Eds., D. O. Thompson and D. E. Chimenti.

Adarsh, K., Soumya, K., Krishnamurthy, C. V. and Krishnan Balasubramaniam, Simultsonic: A Simulation Tool for Ultrasonic Inspection, AIP Conference Proceedings, *Review of Progress in Quantitative Nondestructive Evaluation*, Eds., D. O. Thompson and D. E. Chimenti, to be Published

Gengembre, N. and Lhemery, A. (2000) Pencil Method in Elastodynamics: Application to Ultrasonic Field Computation, *Ultrasonics*, Vol. 38, pp. 495 499.

Ginzel, E. A. and Hotchkiss, F. H. C. (1997) Ultrasonic Beam Profile Modelling, *NDT.net*, Vol. 2, No. 6.

Goswami, P. P., Rudolphi, T. J., Roberts, R. A. and Rizzo, F. J. (1991) Ultrasonic Transmission

through a Curved Interface by the Boundary Element Method, *Review of Progress in Quantitative Non-destructive Evaluation*, Eds. D.O. Thompson and D.E. Chimenti, Vol. 10A, pp. 193-200.

Krautkrämer, A. J. and Krautkrämer, H. (1990) Ultrasonic Testing of Materials.

Krishnamurthy, C. V., Shankar, M. and Krishnan Balasubramaniam (2005) Patch Element Model for the Evaluation of Displacement Fields within an Elastic Solid from a Non-Contact Immersion Transducer: Application To The 2004 Ultrasonic Benchmark Problem, *AIP Conference Proceedings CP-760, Review of Progress in Quantitative Non-destructive Evaluation*, Eds. D. O. Thompson and D. E. Chimenti, Vol. 24 B, pp. 1864-1871.

Porter, M. B. (1997) Modeling Sound Propagation in the Ocean, *Computational Wave Propagation*, Eds. B. Engquist and G. A. Kriegsmann.

Rossi, J. P., Levy, A. J. (1992), A Ray Model for Decimetric Radiowave Propagation in an Urban Area, *Radio Science*, Vol. 27, No. 6, pp. 971-979.

Schmerr, L. W., Song, S. J. and Zhang, H. (1994) Model-Based Calibration of Ultrasonic System Responses for Quantitative Measurements, *Nondestructive Characterization of Materials*, VI, Eds., R. E. Green Jr., K. J. Kozaczek, and C. O. Ruud, Plenum Press, N. Y., pp. 111-118.

Schmerr, L. W. (1998) Fundamentals of Ultrasonic Non-Destructive Evaluation: A Modeling Approach.

Schmerr, L. W. (2000) A Multi-Gaussian Ultrasonic Beam Model for High Performance Simulations on a Personal Computer, *Materials Evaluation*, 58, pp. 882-888.